JOURNAL OF MOLECULAR SPECTROSCOPY 172, 282–295 (1995)

Identification and Analysis of the Far-Infrared Laser Magnetic Resonance Spectrum of the HS_2 Radical[1]

STEPHEN H. ASHWORTH,*,[2] KENNETH M. EVENSON,* AND JOHN M. BROWN†

*Time and Frequency Division, National Institute of Standards and Technology (NIST), 325 Broadway, Boulder, Colorado 80303; and †Physical Chemistry Laboratory, South Parks Road, Oxford OX1 3QZ, United Kingdom

The first observation of the far-infrared laser magnetic resonance spectrum of the HS_2 radical in its ground $^2A''$ state is reported. The radical was produced in the gas-phase reaction between fluorine atoms and hydrogen sulfide, H_2S. Spectra associated with several different rotational transitions (with values of N up to 30 and K_a up to 4) have been identified and analyzed to give an improved set of molecular parameters. In particular, the value for the centrifugal distortion constant Δ_K of 24.339(10) MHz is significantly different from the value assumed by S. Yamamoto and S. Saito (*Can. J. Phys.* **72**, 954 (1994)) in their earlier millimeter-wave study. Zeeman parameters have also been determined.

INTRODUCTION

Much effort has been put into the investigation of the HO_2 radical, both from the point of view of its spectroscopy (*1, 2*) and also its kinetics (*3*). This is understandable given the importance of the HO_2 radical in both atmospheric and combustion chemistry. Its sulfur analog, the HS_2 radical, has received scant attention by comparison. This may be due in part to the difficulties inherent in the detection of the spectrum of a heavy asymmetric-top free radical. Not only is the steady state concentration of a short-lived radical in the detection region likely to be low but also the total spectral intensity is spread over a large number of rotational lines.

The first spectroscopic observations on HS_2 were made in 1950 when a transient, diffuse band system was observed in absorption between 315 and 380 nm in a flash kinetic experiment on H_2S (*4*); this band system has not yet been assigned. The $\tilde{A}^2A' \leftarrow \tilde{X}^2A''$ system at 1.30 μm has also been recorded in emission at rather low resolution (*5*) and a number of vibrational constants have been determined. The band contour analysis of these observations was based upon the previous theoretical work of Sannigrahi *et al.* (*6*). Recently, the millimeter-wave spectra of the HS_2 and DS_2 radicals have been reported (*7*) and compared with further *ab initio* calculations (*8*). In the present work we have identified a contaminant spectrum in an earlier study of the SH radical (*9*) as being due to the HS_2 radical. This has allowed us to make further observations of HS_2 throughout the 305- to 170-μm region. The observed resonances have been modeled with an asymmetric-top effective Hamiltonian to derive a set of parameters for HS_2 in the $\tilde{X}^2A''$ state. These parameters are discussed with respect to the structure of the HS_2 radical and its analogs.

[1] Work supported in part by NASA Contract W-18,623.

[2] Present Address: Max-Born Institut, Rudower Chaussee 6, 12489 Berlin, Germany.

0022-2852/95 $12.00

EXPERIMENTAL DETAILS

The far-infrared laser magnetic resonance (LMR) spectra were recorded at the Boulder laboratories of NIST using an LMR spectrometer which has been slightly modified from that described previously (*10*). In the present spectrometer the output power was coupled from the beamsplitter, which divides the sample region from the laser gain region. The arrangement is shown in Fig. 1. The beamsplitter is held taut, in the central region only, by a metal frame. The frame can be rotated through a few degrees so that the outcoupled power may be adjusted. An external mirror is attached to the spindle on which the beamsplitter is rotated and held at 90° to it. This keeps the outcoupled beam parallel to the axis during adjustment.

The HS_2 radicals were produced continuously in the detection region by the reaction of H_2S with fluorine atoms. The fluorine atoms were created in a microwave discharge in 400 mTorr (0.53 Pa) of 5% fluorine in helium diluent. The reaction region was wrapped with heater tape to prevent sulfur deposits forming on the walls of the cell in the vicinity of the gas input. In most cases warming the cell walls enhanced the signal-to-noise ratio.

The maximum signal-to-noise ratio was around 500:1 with an output time constant of 0.3 sec. Under these conditions quartets were observed, which are probably due to ^{33}S nuclear hyperfine structure ($I = \frac{3}{2}$) in HS_2 isotopomers containing one ^{33}S atom, present in natural abundance (0.75%).

The magnet used was a 15-in. Varian electromagnet capable of generating a flux density of up to 1.8 T. The Zeeman modulation was applied using a pair of Helmholtz coils strapped to the sides of the sample region. The magnetic flux densities were measured with a Hall probe which was calibrated with an NMR gaussmeter.

OBSERVATIONS

The transitions observed in the present study are summarized in Table I together with the laser lines used. All the observations were made in π polarization; thus ΔM_J

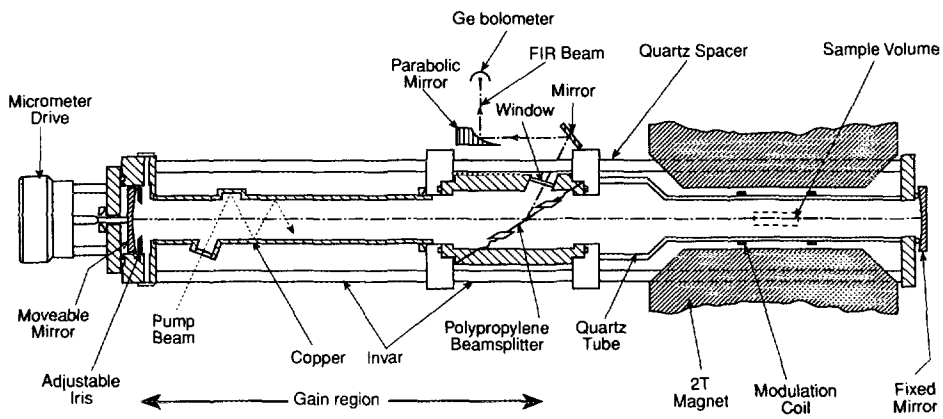

FIG. 1. A cross-sectional view of the far-infrared LMR spectrometer used in this work. The lasing gas is confined to the left-hand portion of the laser cavity by the polypropylene beamsplitter which is adjusted close to Brewster's angle. The sample of HS_2 gas is generated in the center of a large electromagnet in the right-hand portion of the cavity. A small fraction of the laser power is coupled out through reflection off the surface of the beamsplitter and is focused onto a bolometer detector.

TABLE I

Summary of Transitions Observed in the Far-Infrared Spectrum of HS_2 by LMR

		Laser line		
Assignment	Frequency/GHz	Pump	λ/μm	Gas
$6_{24} - 5_{15}$	980.5916	9R(8)	305.7	CH_3OD
$8_{27} - 7_{16}$	980.5916	9R(8)	305.7	CH_3OD
$10_{29} - 9_{18}$[a]	1016.8972	9R(8)	294.8	CH_3OD
~[b]	1338	9R(34)	224.0[c]	$^{13}CH_2F_2$
$30_{2,28} - 29_{1,29}$	1385.6461	10P(24)	216.4	$^{13}CD_3OD$
$30_{2,28} - 29_{1,29}$	1397.1186	9R(34)	214.6	CH_2F_2
$5_3 - 5_2$[d]	1419.0493	10R(4)	211.3	CH_3OH
$3_{31} - 3_{22}$	1472.1994	10R(16)	203.6	$^{13}CH_3OH$
$11_{39} - 10_{28}$	1632.6669	9P(10)	183.4	CH_2DOH
$15_{3,12} - 14_{2,13}$	1668.0350	10R(4)	179.7	CH_3OH
$22_{4,18} - 23_{3,21}$	1668.0350	10R(4)	179.7	CH_3OH
$22_{4,19} - 23_{3,20}$	1668.0350	10R(4)	179.7	CH_3OH
$10_{47} - 11_{38}$	1821.3352	9P(16)	164.6	CH_3OH

[a] Transition assigned but not included in the fit.

[b] These spectra are attributed to HS_2 on the basis of chemical behavior and the characteristics of the spectra.

[c] Laser line not previously reported. Wavelength measured from micrometer calibrated with known transition.

[d] K-doubling not resolved.

= 0 transitions were observed. Without exception, the spectra are far more complex than this table suggests. Only the features forming obvious series of lines received detailed attention. The complexity can be seen in Fig. 2 where the high field region of the 179.7-μm survey scan is shown. There are four series of strong lines which have been assigned. In addition there are many weaker signals, mostly at lower flux densities. These were not assigned and many are probably due to the isotopomers of HS_2 (^{32}S, 95.02%; ^{33}S, 0.75%; ^{34}S, 4.21%).

We were able to resolve the K-doubling in all of the recorded spectra except the 164-μm spectrum where the tuning rate was low (i.e., the spectral lines were broad) and the K-doubling was relatively small. In Fig. 2 the doublets at high field assigned to the $N = 22 \leftarrow 23$ $K = 4 \leftarrow 3$ transition are K-doublets. In favorable cases the proton hyperfine splitting was almost completely resolved. This can be seen in Fig. 3, where part of the 179.7-μm spectrum is expanded.

The hyperfine splitting is also obvious in Fig. 4 where a single Zeeman "branch" is shown. This is the spin-state partner to the original observations of a contaminant spectrum in the far-infrared LMR spectrum of SH (*9*). Unfortunately, the original observations were not repeated because the laser line required could not be made to oscillate. Some of the additional signals may be due to other species in the discharge. However, small leaks in the vacuum system occurred from time to time and usually had a marked effect on the appearance of the spectrum. The effect on the chemistry in the sample region was confirmed by adding small amounts of oxygen below the discharge region. In these cases we might expect species such as HSO, SO, and possibly HOS, HO_2, or FO to be formed. We were able to distinguish between these oxygen-bearing species and the spectra due to HS_2 by such chemical tests.

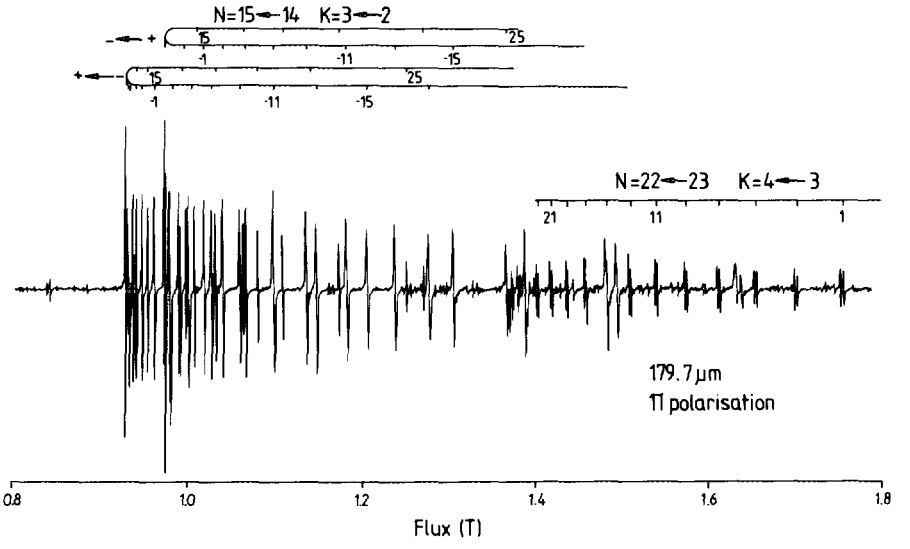

FIG. 2. A portion of the far-infrared LMR spectrum of the HS_2 radical in its ground $^2A''$ state recorded with the 179.7-μm laser line of CH_3OH in π-polarization ($\Delta M_J = 0$). The difference in K-doubling between the $K = 3$–2 and $K = 4$–3 subbands can clearly be seen. The numbers on the grids denote the values of the M_J quantum number assigned to the individual transitions ($2M_J$).

ANALYSIS AND LEAST-SQUARES FIT

In many earlier studies by LMR, the spectra have been assigned in a relatively straightforward fashion, using previously determined parameters and a predictive computer program. In this case, however, the previous work in the millimeter-wave region (*7*) was not extensive enough to determine the $\Delta K_a = +1$ subband origins accurately. Only $K_a = 1$–0 transitions had been detected so it was not possible to determine the parameter Δ_K. This parameter was absorbed into the A rotational con-

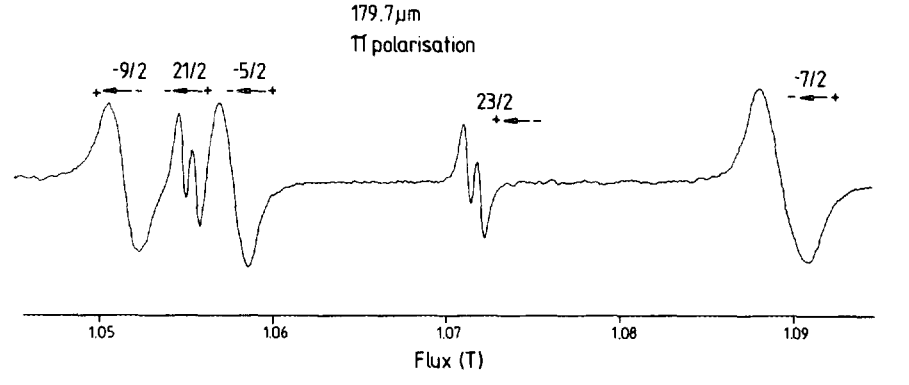

FIG. 3. An expanded view of part of the far-infrared LMR spectrum of the HS_2 radical in its ground $^2A''$ state recorded with the 179.7-μm laser line of CH_3OH in π-polarization ($\Delta M_J = 0$). The numbers in the figure denote the M_J values assigned to the individual transitions. The $M_J = \frac{23}{2}$ and $M_J = \frac{21}{2}$ signals show a small doubling which arises from the proton hyperfine structure. This structure is not resolved in the broader signals.

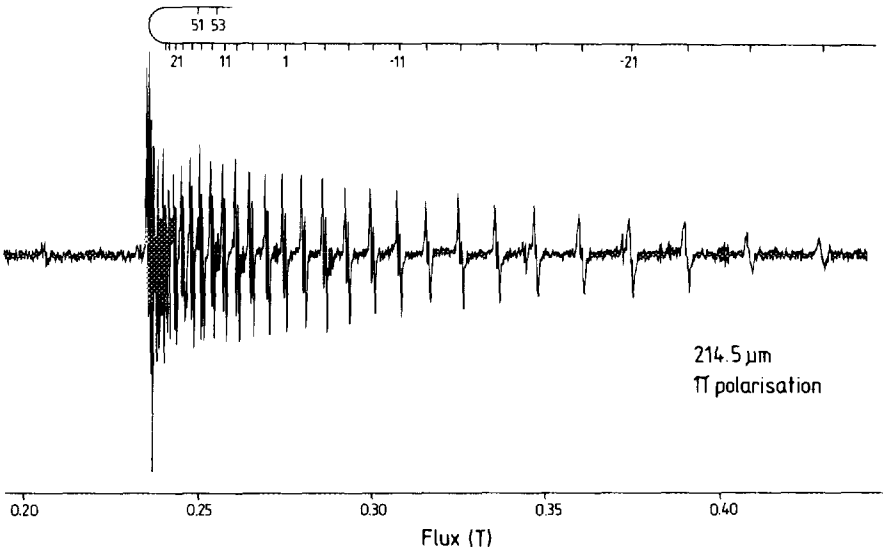

FIG. 4. A portion of the far-infrared LMR spectrum of the HS_2 radical in its ground $^2A''$ state recorded with the 214.58-μm laser line of CH_2F_2 in π-polarization ($\Delta M_J = 0$). The numbers on the grid denote the values of $2M_J$ assigned to the individual transitions.

stant which was therefore $A_{\text{eff}} = A - \Delta_K$. Predictions of the K-subband origins with these parameters would, therefore, become increasingly unreliable with increasing K.

The initial predictions of the zero-field spectrum of HS_2 in the far-infrared region were carried out with a value of $\Delta_K = 25$ MHz, estimated from the values for HO_2 (*11*) and HSO (*12*). When an appropriately close coincidence between a molecular transition frequency and a laser frequency had been chosen, a prediction of the Zeeman pattern was made. The g-factors required were estimated from the expressions

$$g_S^{\alpha\alpha} = g_S - \frac{\epsilon_{\alpha\alpha}}{2B_{\alpha\alpha}} \tag{1}$$

$$g_\tau^{\alpha\alpha} = \frac{-|\epsilon_{\alpha\alpha}|}{\zeta}, \tag{2}$$

in the standard notation (*13*). The parameter ζ was taken to be 382 cm^{-1}, the spin–orbit coupling constant of atomic sulfur (*14*). After a tentative assignment had been made, the M_J values were assigned for individual transitions. In the present work this was complicated because of the nonlinearity of the Zeeman effect. It can be seen in both Figs. 2 and 4 that the Zeeman branches form heads. We used two different methods to assist in the assignment. The first was a simple graphical method. The variation of molecular transition frequency with applied field was calculated and plotted. The expected Zeeman patterns and their dependence on the difference between the calculated zero-field frequency and the laser frequency can be easily seen. The second method was that developed by Hougen for the analysis of the LMR spectrum of the HO_2 radical (*15*). This involves fitting trial M_J values to a simple quadratic expression in M_J and flux density. The variable parameters may be related to molecular splittings but this was not necessary for the present work. This approach was applied successfully to the analysis of the far-infrared spectrum of HO_2. In the present work,

TABLE IIa

Results of the Refit of the Millimeter-Wave Data of the HS_2 Radical in the (0, 0, 0) Vibrational Level of the Ground $\tilde{X}^2A''$ State

$N_{K_aK_c} \leftarrow N_{K_aK_c}$	$2J'$	$2J''$	F'	F''	Frequency[a]	$\Delta\nu$[b]
$9_{0,9} - 8_{0,8}$	19	17			141.824148	8
$9_{0,9} - 8_{0,8}$	17	15			142.025731	17
$9_{1,9} - 8_{1,8}$	19	17			141.453887	12
$9_{1,9} - 8_{1,8}$	17	15			140.325661	39
$9_{1,8} - 8_{1,7}$	19	17			143.312745	12
$9_{1,8} - 8_{1,7}$	17	15			142.398631	35
$9_{2,8} - 8_{2,7}$	19	17			143.524816	-8
$9_{2,8} - 8_{2,7}$	17	15			140.040187	34
$9_{2,7} - 8_{2,6}$	19	17			143.537000	-20
$9_{2,7} - 8_{2,6}$	17	15			140.057027	1
$9_{3,7} - 8_{3,6}^c$	19	17			144.616794	10
$9_{3,7} - 8_{3,6}^c$	17	15			138.855297	9
$9_{3,6} - 8_{3,5}^c$	19	17			144.616771	-28
$9_{3,6} - 8_{3,5}^c$	17	15			138.855323	10
$10_{0,10} - 9_{0,9}$	21	19			157.585782	-13
$10_{0,10} - 9_{0,9}$	19	17			157.785933	12
$10_{1,10} - 9_{1,9}$	21	19			157.016913	7
$10_{1,10} - 9_{1,9}$	19	17			156.101436	15
$10_{1,9} - 9_{1,8}$	21	19			159.096099	-10
$10_{1,9} - 9_{1,8}$	19	17			158.394683	5
$10_{2,9} - 9_{2,8}$	21	19			159.059317	-7
$10_{2,9} - 9_{2,8}$	19	17			156.083319	24
$10_{2,8} - 9_{2,7}$	21	19			159.076465	-14
$10_{2,8} - 9_{2,7}$	19	17			156.106186	-23
$10_{3,8} - 9_{3,7}^c$	21	19			160.083668	-39
$10_{3,8} - 9_{3,7}^c$	19	17			154.956764	-13
$10_{3,7} - 9_{3,6}^c$	21	19			160.083694	-38
$10_{3,7} - 9_{3,6}^c$	19	17			154.956806	-12
$10_{4,6} - 9_{4,5}^c$	21	19			160.914570	-33
$10_{4,6} - 9_{4,5}^c$	19	17			154.047397	6
$15_{0,15} - 14_{0,14}$	31	29			236.349920	-25
$15_{0,15} - 14_{0,14}$	29	27			236.536045	11
$15_{1,15} - 14_{1,14}$	31	29			235.025973	-3
$15_{1,15} - 14_{1,14}$	29	27			234.649466	27
$15_{1,14} - 14_{1,13}$	31	29			238.212048	-2
$15_{1,14} - 14_{1,13}$	29	27			238.038257	-16
$15_{2,14} - 14_{2,13}$	31	29			237.166267	-17
$15_{2,14} - 14_{2,13}$	29	27			235.696887	-4
$15_{2,13} - 14_{2,12}$	31	29			237.228381	3
$15_{2,13} - 14_{2,12}$	29	27			235.771857	-17
$15_{3,12} - 14_{3,11}^c$	31	29			237.867692	-1
$15_{3,12} - 14_{3,11}^c$	29	27			234.906829	-13
$15_{3,13} - 14_{3,12}^c$	31	29			237.867472	-1
$15_{3,13} - 14_{3,12}^c$	29	27			234.906523	-16
$15_{4,11} - 14_{4,10}^c$	31	29			238.532480	-22
$15_{4,11} - 14_{4,10}^c$	29	27			234.100608	-14
$15_{5,11} - 14_{5,10}^c$	31	29			239.112270	-33
$15_{5,11} - 14_{5,10}^c$	29	27			233.376872	-7
$16_{0,16} - 15_{0,15}$	33	31			252.092065	-43
$16_{1,16} - 15_{1,15}$	33	31			250.643925	12
$16_{1,16} - 15_{1,15}$	31	29			250.322274	43
$16_{2,15} - 15_{2,14}$	33	31			252.837520	25
$16_{2,15} - 15_{2,14}$	31	29			251.543387	-17
$16_{2,14} - 15_{2,13}$	33	31			252.913477	18
$16_{2,14} - 15_{2,13}$	31	29			251.634025	3
$16_{3,14} - 15_{3,13}^c$	33	31			253.486772	6
$16_{3,14} - 15_{3,13}^c$	31	29			250.813170	-9
$16_{3,13} - 15_{3,12}^c$	33	31			253.487080	4
$16_{3,13} - 15_{3,12}^c$	31	29			250.813588	-8
$16_{4,13} - 15_{4,12}^c$	31	29			250.038201	2
$16_{5,11} - 15_{5,10}^c$	31	29			249.324765	-7
$17_{0,17} - 16_{0,16}$	35	33			267.830064	-40
$17_{0,17} - 16_{0,16}$	33	31			267.992721	-27
$17_{1,17} - 16_{1,16}$	35	33			266.263175	-41
$17_{1,17} - 16_{1,16}$	33	31			265.987330	25
$17_{1,16} - 16_{1,15}$	35	33			269.952169	27
$17_{1,16} - 16_{1,15}$	33	31			269.812618	4
$17_{2,16} - 16_{2,15}$	35	33			268.517494	-9
$17_{2,16} - 16_{2,15}$	33	31			267.373536	3
$17_{2,15} - 16_{2,14}$	35	33			268.609278	34
$17_{2,15} - 16_{2,14}$	33	31			267.481836	30
$17_{3,14} - 16_{3,13}^c$	35	33			269.120237	14
$17_{3,14} - 16_{3,13}^c$	33	31			266.700070	-35
$17_{3,15} - 16_{3,14}^c$	35	33			269.119813	15
$17_{3,15} - 16_{3,14}^c$	33	31			266.699508	-35
$17_{4,13} - 16_{4,12}^c$	35	33			269.706377	20
$17_{4,13} - 16_{4,12}^c$	33	31			265.955688	2
$17_{5,13} - 16_{5,12}^c$	35	33			270.240419	9
$17_{5,13} - 16_{5,12}^c$	33	31			265.255055	9
$18_{0,18} - 17_{0,17}$	37	35			283.563668	-5
$18_{0,18} - 17_{0,17}$	35	33			283.671871	-16
$18_{1,18} - 17_{1,17}$	37	35			281.882906	-10
$18_{1,18} - 17_{1,17}$	35	33			281.645597	47
$18_{1,17} - 17_{1,16}$	37	35	19	18	286.725847	-29
$18_{1,17} - 17_{1,16}$	36	34	18	17	286.720463	-24
$18_{1,17} - 17_{1,16}$	35	33			285.688755	-21
$18_{2,17} - 17_{2,16}$	37	35			284.204186	-13
$18_{2,17} - 17_{2,16}$	35	33			283.189544	-12
$18_{2,16} - 17_{2,15}$	37	35			284.313781	37
$18_{2,16} - 17_{2,15}$	35	33			283.317621	-1
$18_{3,16} - 17_{3,15}^c$	37	35			284.764302	10
$18_{3,16} - 17_{3,15}^c$	35	33			282.568019	14
$18_{3,15} - 17_{3,14}^c$	37	35			284.764874	10
$18_{3,15} - 17_{3,14}^c$	35	33			282.568764	14
$18_{4,15} - 17_{4,14}^c$	37	35			285.312623	22
$18_{4,15} - 17_{4,14}^c$	35	33			281.854727	-10
$18_{5,13} - 17_{5,12}^c$	37	35			285.821660	22
$18_{5,13} - 17_{5,12}^c$	35	33			281.168623	9
$19_{0,19} - 18_{0,18}$	38	36	19	18	298.462549	22
$19_{0,19} - 18_{0,18}$	37	35	18	17	298.467892	24
$19_{1,18} - 18_{1,17}$	38	36	19	18	300.171655	-18
$4_{1,3} - 4_{0,4}$	8	8	4	4	302.145473	9
$4_{1,3} - 4_{0,4}$	7	7	3	3	302.147377	-43
$5_{1,4} - 5_{0,5}$	10	10	5	5	300.891487	14
$5_{1,4} - 5_{0,5}$	9	9	4	4	300.893288	32
$6_{1,5} - 6_{0,6}$	12	12	6	6	300.215405	1
$6_{1,5} - 6_{0,6}$	11	11	5	5	300.217012	-16
$7_{1,6} - 7_{0,7}$	14	14	7	7	299.972179	16
$7_{1,6} - 7_{0,7}$	13	13	6	6	299.973651	-6
$8_{1,7} - 8_{0,8}$	16	16	8	8	300.067859	9
$8_{1,7} - 8_{0,8}$	15	15	7	7	300.069242	1
$9_{1,8} - 9_{0,9}$	18	18	9	9	300.440775	5
$9_{1,8} - 9_{0,9}$	17	17	8	8	300.442089	8
$10_{1,9} - 10_{0,10}$	20	20	10	10	301.049559	2

TABLE IIa—*Continued*

$N_{K_aK_c} \leftarrow N_{K_aK_c}$	$2J'$	$2J''$	F'	F''	Frequency[a]	$\Delta\nu$[b]
$10_{1,9} - 10_{0,10}$	19	19	9	9	301.050809	3
$11_{1,10} - 11_{0,11}$	22	22	11	11	301.865944	12
$11_{1,10} - 11_{0,11}$	21	21	10	10	301.867134	2
$12_{1,11} - 12_{0,12}$	24	24	12	12	302.870246	-21
$12_{1,11} - 12_{0,12}$	23	23	11	11	302.871427	-2
$4_{1,3} - 4_{0,4}$	9	9	5	5	280.023298	50
$4_{1,3} - 4_{0,4}$	8	8	4	4	280.022622	19
$5_{1,4} - 5_{0,5}$	11	11	6	6	281.890120	24
$5_{1,4} - 5_{0,5}$	10	10	5	5	281.889446	-13
$6_{1,5} - 6_{0,6}$	13	13	7	7	283.550110	-15
$6_{1,5} - 6_{0,6}$	12	12	6	6	283.549496	-5
$7_{1,6} - 7_{0,7}$	15	15	8	8	285.097324	-11
$7_{1,6} - 7_{0,7}$	14	14	7	7	285.096729	5
$8_{1,7} - 8_{0,8}$	17	17	9	9	286.593999	-14
$8_{1,7} - 8_{0,8}$	16	16	8	8	286.593397	-14
$10_{1,9} - 10_{0,10}$	21	21	11	11	289.592914	3
$10_{1,9} - 10_{0,10}$	20	20	10	10	289.592266	-54
$11_{1,10} - 11_{0,11}$	23	23	12	12	291.146560	-0
$11_{1,10} - 11_{0,11}$	22	22	11	11	291.145945	-29
$12_{1,11} - 12_{0,12}$	25	25	13	13	292.759774	-9
$12_{1,11} - 12_{0,12}$	24	24	12	12	292.759172	-30
$18_{1,17} - 18_{0,18}$	36	36	18	18	305.324565	16
$18_{1,17} - 18_{0,18}$	37	37	19	19	305.330486	39
$19_{1,18} - 19_{0,19}$	39	39	20	20	306.205052	8
$19_{1,18} - 19_{0,19}$	38	38	19	19	306.203695	-2

[a] Frequency given in GHz.
[b] Observed-calculated frequency given in kHz.
[c] Frequency adjusted to reproduce the K-doubling and weight adjusted accordingly (see text).

the best quadratic fit gave M_J values which were at most ± 1 unit from those used in the final assignment.

The preliminary work concentrated on the lowest frequency spectrum, recorded with the 305.7-μm laser line, because the extrapolation from the available parameters would be most reliable at low K. The two spectra observed on this line were assigned, using the techniques outlined above. Having assigned the transitions, we were able to fit our data together with the millimeter-wave data. Thus a reliable value for Δ_K was determined and the g-factors refined. With this revised parameter set, extending the predictions and assigning the higher K transitions were both relatively straightforward.

The predictions and least-squares fitting of the data were both carried out using a computer program which was developed by Brown and Sears (*16*) and which has been placed in the public domain as ASYTOP. At high N and K, the program dimensions were too small to handle the optimum basis set, so minor changes to the code were made to expand the maximum size of the basis set. The effective Hamiltonian used by this program was developed by Bowater *et al.* (*13*), who explain the derivation of the matrix elements and the assumptions inherent therein.

The ASYTOP program allows a specific basis set to be allocated to each data point. This is obviously a more efficient procedure than calculating all eigenvalues with the largest basis set required. In most cases, a basis limited by $\Delta N = \pm 2$ and $\Delta K = \pm 2$, evaluated with both odd and even values of K, was sufficient. At higher N, however, the basis set had to be increased to include $\Delta K = \pm 4$.

The LMR data were fitted together with millimeter-wave data from Yamamoto and Saito (*7*). We found that, although the K-doublets were not resolved in the millimeter-wave experiment above $K = 2$, there was sufficient doubling to skew the fit when only one of the two K-doublets was assigned to the observed frequency. We thus calculated the appropriate doubling and included "dummy" lines in the fit at $K = 3$ so that the center frequency was the observed frequency but the K-doubling was still reproduced. These lines were given half the weight of the other transitions.

Each LMR data point on the other hand was generally given one ten-thousandth of the weight of the millimeter-wave data, reflecting the two orders of magnitude

TABLE IIb

Results of the Fit of LMR Data of the HS_2 Radical in the (0, 0, 0) Vibrational Level of the Ground $\tilde{X}^2A''$ State

$6_{24} - 5_{15}$, $F_2 - F_2$

980.5916 GHz 305.7 μm 9R(8) CH_3OD

M_J[a]	M_I	Flux/T	$\frac{\partial\nu}{\partial B}$[b]	$\Delta\nu$[c]	σ[d]
9/2	1/2	0.74756	−9.0	−0.36	2
7/2	1/2	0.74693	−9.0	0.69	2
9/2	−1/2	0.64526	−7.4	−0.63	2
5/2	1/2	0.64464	−7.4	0.32	2
7/2	−1/2	0.58877	−6.5	−0.14	2
3/2	1/2	0.58811	−6.5	0.54	2
5/2	−1/2	0.55551	−5.9	−2.08	2
1/2	1/2	0.55494	−5.9	−0.87	2
3/2	−1/2	0.53792	−5.4	−1.13	2
−1/2	1/2	0.53712	−5.4	−1.13	2
1/2	−1/2	0.53193	−4.9	−0.86	2
−3/2	1/2	0.53130	−4.9	0.05	2
−1/2	−1/2	0.53688	−4.3	−0.09	2
−5/2	1/2	0.53589	−4.3	−0.79	2
−5/2		0.55296	−3.8	−1.36	2
−7/2		0.58594	−3.2	−1.29	2

$8_{27} - 7_{16}$, $F_1 - F_1$

980.5916 GHz 305.7 μm 9R(8) CH_3OD

M_J[a]	M_I	Flux/T	$\frac{\partial\nu}{\partial B}$[b]	$\Delta\nu$[c]	σ[d]
13/2	1/2	0.91810	14.5	−2.06	2
13/2	−1/2	0.91748	14.5	−3.54	2
11/2	1/2	0.91118	11.9	2.72	2
11/2	−1/2	0.91041	11.9	2.80	2
9/2	1/2	0.92242	10.1	0.76	2
9/2	−1/2	0.92160	10.1	0.88	2
7/2	1/2	0.94736	8.7	2.01	2
7/2	−1/2	0.94657	8.7	1.61	2
5/2	1/2	0.98599	7.5	1.35	2
5/2	−1/2	0.98518	7.5	0.91	2
3/2	1/2	1.03903	6.5	3.50	2
3/2	−1/2	1.03819	6.5	3.16	2
1/2	1/2	1.11059	5.5	1.74	2
1/2	−1/2	1.10978	5.5	1.19	2
−1/2		1.20574	4.6	−2.83	2
−3/2		1.33242	3.8	−1.19	2

$30_{2,28} - 29_{1,29}$, $F_2 - F_2$

1397.1186 GHz 214.6 μm 9R(34) CH_2F_2

M_J[a]	M_I	Flux/T	$\frac{\partial\nu}{\partial B}$[b]	$\Delta\nu$[c]	σ[d]
15/2	−1/2	0.25424	−7.7	−3.43	2
11/2	1/2	0.25347	−7.7	−3.46	2
13/2	−1/2	0.25763	−7.5	−3.80	2
9/2	1/2	0.25686	−7.5	−3.89	2
11/2	−1/2	0.26144	−7.2	−3.66	2
7/2	1/2	0.26074	−7.2	−3.14	2
9/2	−1/2	0.26581	−6.9	−2.20	2
5/2	1/2	0.26504	−6.9	−2.12	2
7/2	−1/2	0.27052	−6.7	−1.11	2
3/2	1/2	0.26972	−6.7	−1.24	2
5/2	−1/2	0.27548	−6.4	−1.28	2
1/2	1/2	0.27475	−6.4	−0.95	2
3/2	−1/2	0.28111	−6.2	−0.16	2
−1/2	1/2	0.28027	−6.2	−0.46	2
1/2	−1/2	0.28717	−5.9	0.48	2
−3/2	1/2	0.28633	−5.9	0.22	2
−3/2		0.29340	−5.7	1.12	2
−5/2		0.30070	−5.4	2.01	2
−7/2		0.30849	−5.2	1.84	2
−9/2		0.31685	−4.9	0.68	2
−11/2		0.32665	−4.7	2.25	2
53/2		0.25548	−15.7	−6.42	2
55/2		0.26261	−17.3	−7.44	2

$5_3 - 5_2$, $F_1 - F_1$

1419.0493 GHz 211.3 μm 10R(4) CH_3OH

M_J[a]	M_I	Flux/T	$\frac{\partial\nu}{\partial B}$[b]	$\Delta\nu$[c]	σ[d]
−9/2		0.42619	0.4	−0.83	2
−7/2		0.34468	0.5	−1.42	2
−5/2		0.30787	0.6	−1.47	2
5/2		0.32168	0.6	−1.32	2
7/2		0.36966	0.6	−0.88	2
9/2		0.47944	0.5	1.70	2

$11_{39} - 10_{28}$, $F_2 - F_2$

1632.6669 GHz 183.4 μm 9P(10) CH_2DOH

M_J[a]	M_I	Flux/T	$\frac{\partial\nu}{\partial B}$[b]	$\Delta\nu$[c]	σ[d]
19/2	−1/2	1.46493	−6.4	1.22	2
15/2	1/2	1.46412	−6.4	1.32	2
19/2	−1/2	1.47480	−6.5	3.36	2
15/2	1/2	1.47389	−6.5	2.82	2
17/2	−1/2	1.35038	−5.6	0.59	2
13/2	1/2	1.34954	−5.6	0.65	2
17/2	−1/2	1.36176	−5.6	1.01	2
13/2	1/2	1.36065	−5.6	−0.51	2
15/2	−1/2	1.28431	−5.1	0.54	2
11/2	1/2	1.28345	−5.1	0.49	2
15/2	−1/2	1.27162	−5.0	0.69	2
11/2	1/2	1.27072	−5.0	0.45	2
13/2	−1/2	1.22929	−4.7	0.56	2
9	1/2	1.22843	−4.7	0.55	2
11/2		1.22886	−4.7	0.56	2
−9/2		1.22551	−2.3	0.93	2
−11/2		1.23989	−2.1	0.74	2
−11/2		1.27412	−2.1	0.85	2
−13/2		1.29984	−1.9	0.62	2
−13/2		1.33887	−1.8	1.04	2
−15/2		1.42593	−1.6	1.48	2
−15/2		1.38044	−1.6	0.67	2

$3_{31} - 3_{22}$, $F_2 - F_2$

1472.1994 GHz 203.6 μm 10R(16) $^{13}CH_3OH$

M_J[a]	M_I	Flux/T	$\frac{\partial\nu}{\partial B}$[b]	$\Delta\nu$[c]	σ[d]
−5/2		0.04045	1.9	−1.94	3
−3/2		0.07014	1.0	−1.65	3

TABLE IIb—*Continued*

$15_{3,12} - 14_{2,13}$, $F_1 - F_1$

1668.0350 GHz 179.7 μm 10R(4) CH_3OH

M_J[a]	M_I	Flux/T	$\frac{\partial\nu}{\partial B}$[b]	$\Delta\nu$[c]	σ[d]
3/2		0.92917	3.9	−1.35	2
13/2		0.93230	5.0	−2.10	2
1/2		0.93933	3.7	−1.77	2
−1/2		0.95243	3.4	0.29	2
3/2		0.98060	3.9	−0.54	2
15/2	1/2	0.98325	5.4	−1.17	2
15/2	−1/2	0.98248	5.4	−1.50	2
19/2	1/2	0.98956	6.0	−2.16	2
19/2	−1/2	0.98879	6.0	−2.45	2
1/2		0.99282	3.7	2.47	2
17/2	1/2	0.99957	5.8	−0.50	2
17/2	−1/2	0.99880	5.8	−0.82	2
−1/2		1.01047	3.5	0.14	2
−7/2		1.01898	2.8	0.17	2
−3/2		1.03180	3.2	0.30	2
−9/2		1.05151	2.6	0.77	2
21/2	1/2	1.05559	6.7	−1.34	2
21/2	−1/2	1.05469	6.7	−0.71	2
−5/2		1.05771	3.0	1.38	2
23/2	1/2	1.07223	7.1	−1.38	2
23/2	−1/2	1.07154	7.1	−2.14	2
23/2	1/2	1.10100	7.4	−2.06	2
23/2	−1/2	1.10021	7.4	−2.07	2
−9/2		1.12805	2.6	1.52	2
−13/2		1.13917	2.2	1.58	2
25/2	1/2	1.16568	8.5	0.46	2
25/2	−1/2	1.16491	8.5	0.38	2
−11/2		1.17447	2.4	1.88	2
−15/2		1.19830	2.0	1.63	2
−13/2		1.23105	2.1	1.83	2
−17/2		1.27133	1.7	2.20	2
−15/2		1.30032	1.9	1.94	2

$10_{47} - 11_{38}$, $F_1 - F_1$

1821.3352 GHz 164.6 μm 9P(16) CH_3OH

M_J[a]	M_I	Flux/T	$\frac{\partial\nu}{\partial B}$[b]	$\Delta\nu$[c]	σ[d]
13/2		0.43820	1.1	0.02	2
11/2		0.44875	1.1	−0.54	2
9/2		0.46056	1.2	0.71	2
7/2		0.47695	1.2	0.19	2
5/2		0.49694	1.2	−0.45	2
3/2		0.52036	1.1	−0.34	2
−1/2		0.58291	1.1	0.26	2
−3/2		0.62578	1.1	−0.02	2
−5/2		0.67884	1.0	0.10	2
−7/2		0.74723	1.0	−0.48	2
−9/2		0.83593	0.9	−0.47	2
−11/2		0.95575	0.9	−0.39	2
−13/2		1.12158	0.8	0.04	2

$22_4 - 23_3$, $F_2 - F_2$

1668.0350 GHz 179.7 μm 10R(4) CH_3OH

M_J[a]	M_I	Flux/T	$\frac{\partial\nu}{\partial B}$[b]	$\Delta\nu$[c]	σ[d]
19/2		1.43468	−4.9	−8.29	0
19/2		1.43686	−4.9	−8.09	0
17/2		1.45641	−4.7	−9.07	0
17/2		1.45863	−4.7	−9.17	0
15/2		1.48132	−4.4	−8.98	0
15/2		1.48331	−4.4	−10.61	0
13/2		1.50928	−4.2	−9.35	0
13/2		1.51190	−4.2	−8.74	0
11/2		1.54010	−4.0	−11.66	0
11/2		1.54271	−4.0	−11.65	0
9/2		1.57459	−3.8	−13.51	0
9/2		1.57739	−3.8	−13.29	0
7/2		1.61324	−3.6	−14.24	0
7/2		1.61608	−3.6	−14.45	0
5/2		1.65631	−3.4	−14.50	0
5/2		1.65929	−3.4	−14.78	0
3/2		1.70347	−3.2	−16.86	0
3/2		1.70673	−3.2	−16.84	0
1/2		1.75635	−3.0	−17.75	0
1/2		1.75983	−3.0	−17.68	0

$30_{2,28} - 29_{1,29}$, $F_1 - F_1$

1385.6461 GHz 216.4 μm 10P(25) $^{13}CD_3OD$

M_J[a]	M_I	Flux/T	$\frac{\partial\nu}{\partial B}$[b]	$\Delta\nu$[c]	σ[d]
33/2	1/2	0.29801	11.6	1.00	5
33/2	−1/2	0.29720	11.6	1.64	5
31/2	1/2	0.30063	11.2	0.89	5
31/2	−1/2	0.29988	11.2	0.89	5
29/2	1/2	0.30357	10.7	1.27	5
29/2	−1/2	0.30282	10.7	1.23	5
27/2	1/2	0.30694	10.3	0.98	5
27/2	−1/2	0.30593	10.3	3.70	5
25/2	1/2	0.31074	10.0	0.19	5
25/2	−1/2	0.30999	10.0	0.12	5
23/2	1/2	0.31486	9.6	0.09	5
23/2	−1/2	0.31411	9.6	0.00	5
19/2	1/2	0.32406	8.9	2.28	5
19/2	−1/2	0.32332	8.9	2.10	5
17/2	1/2	0.32942	8.5	2.37	5
17/2	−1/2	0.32868	8.5	2.17	5

[a] All transitions $\Delta M_J = 0$ and $\Delta I = 0$.

[b] Tuning rate given in MHz/mT.

[c] Observed-calculated frequency given in MHz.

[d] Uncertainty of measurement (MHz). An uncertainty of 0 implies zero weight in the fit.

TABLE III

Molecular Parameters of the HS_2 Radical in the (0, 0, 0) Vibrational Level of the Ground $\tilde{X}^2A''$ Electronic State

Parameter	Value[a]	Parameter	Value[a]
A	296.979060(13)[b]	Φ_N	0.0[c]
B	7.9963819(47)	Φ_{NK}	0.0[c]
C	7.7767198(48)	$\Phi_{KN} \times 10^7$	0.321(12)
$\Delta_N \times 10^5$	0.588684(62)	$\Phi_K \times 10^5$	0.832(61)
$\Delta_{NK} \times 10^3$	0.233573(30)	ϕ_N	0.0[c]
Δ_K	0.024339(10)	ϕ_{NK}	0.0[c]
$\delta_N \times 10^6$	0.15580(28)	ϕ_K	0.0[c]
$\delta_K \times 10^3$	0.1390(24)	L_K	0.0[c]
ϵ_{aa}	−45.926824(34)	$\Delta^s_{NK} \times 10^4$	−0.6261(75)
ϵ_{bb}	−0.4240583(83)	$\Delta^s_N \times 10^6$	0.216(14)
ϵ_{cc}	0.0098204(90)	$\delta^s_K \times 10^4$	0.0[c]
$\frac{1}{2}\lvert\epsilon_{ab} + \epsilon_{ba}\rvert$	0.2346966(49)	Φ^S_K	0.0[c]
$\Delta^s_K \times 10^2$	0.6429(22)	δ^s_N	0.0[c]
$\frac{1}{2}(\Delta^s_{NK} + \Delta^s_{KN}) \times 10^3$	−0.64979[c]		
$(0)_H$	−0.02260(15)	$(ab)_H$	−0.001783(26)
$(aa)_H$	−0.00598(15)	$(bb)_H$	0.005892(30)
g_S^{aa}	2.07809(47)	$g_r^{aa} \times 10^3$	−3.996(66)[d]
g_S^{bb}	2.0295(11)	$g_r^{bb} \times 10^3$	−0.054810[d]
g_S^{cc}	2.0013(11)	$g_r^{cc} \times 10^3$	−0.018476[d]
g_N	5.5856912[c]		

[a] Parameter value in GHz where appropriate.

[b] Figures in parentheses are one standard deviation of the least-squares fit given in units of the last quoted decimal place.

[c] Parameter constrained to this value in the fit.

[d] Parameter calculated from tensor (see text).

lower accuracy of the data. Some transitions included in the fit were given even lower weights depending on the recordings which were used to make the measurements. We were unable to reproduce the original data because the appropriate laser line at 214.5 μm could not be made to oscillate; a few transitions, from an earlier recording, have been therefore included. These were weighted an order of magnitude lower than the majority of the data. The results of the fit are given in Tables IIa and IIb.

The 22_4–23_3 transitions were included in the fit at zero weight (see Table IIb). In spite of much effort, we are unable to suggest why these transitions fit so badly (residuals of 10 to 15 MHz). We are confident of the assignment because there are no other suitable transitions in that spectral region and the K-doubling is reproduced very well. An examination of the assignment rules out a local perturbation from levels differing in N or K by one unit in the same spin component. We have also examined the predicted eigenvalues but found no coincidences. Weighting these transitions and varying additional parameters merely degraded the overall quality of fit.

The parameters obtained are shown in Table III. The parameters quoted are not in all cases those fitted by the ASYTOP program. In the case of $\epsilon_{\alpha\alpha}$, $g_S^{\alpha\alpha}$, $g_r^{\alpha\alpha}$, and the hyperfine parameters, the fit is made to spherical tensor components, which are linear

TABLE IV

A Comparison between Experimental and Calculated Values of the Electron Spin g-Tensor Anisotropies for HS_2

Component	$g_S^{\alpha\alpha}$	$\Delta g_S^{\alpha\alpha}$ [a]	$-\epsilon/2B_{\alpha\alpha}$ [b]
a	2.07809(47)[c]	0.0761	0.0773
b	2.0295(11)	0.0275	0.0265
c	2.0013(11)	-0.0007	-0.0006

[a] The anisotropy $\Delta g_S^{\alpha\alpha}$ is defined as $(g_S^{\alpha\alpha} - g_e)$, where g_e is the isotropic electron spin g-factor which is taken to be 2.0020 (allowing for a small, relativistic correction) in the present calculation.

[b] Estimate of the g-tensor anisotropy from Curl's relationship (*19*).

[c] The figures in parentheses are one standard deviation of the least-squares fit, in units of the last quoted decimal place.

combinations of the quoted parameters. It is, therefore, not possible to constrain any one of these parameters to a particular value in the fit. In this work this consideration only applies to the $g_r^{\alpha\alpha}$ values.

Where parameters have been fitted as linear combinations, such as the tensor components mentioned above, the standard deviations have been calculated as the deviation of the quoted parameter, taking into account the correlation between parameters.

DISCUSSION

In this paper we report the observation and analysis of the far-infrared LMR spectrum of the HS_2 radical in the (0, 0, 0) vibrational level of its ground $\tilde{X}^2A''$ electronic state. This has resulted in the determination of previously undetermined molecular parameters and the refinement of several others.

The millimeter-wave spectrum of the HS_2 free radical has been studied by Yamamoto and Saito (*7*). They observed rotational transitions of both HS_2 and DS_2 and determined an r_z structure from their results: r_z(S–H) = 0.1362(3) nm, r_z(S–S) = 0.19650(7) nm, and α_z(HSS) = 101.7(4)°. They also used vibrationally averaged values from an harmonic force field to derive an r_e structure which they compared with the results of a recent *ab initio* calculation by Zhuo *et al.* (*8*). The agreement was very close. The values of the molecular parameters determined by Yamamoto and Saito agree well with those of the present work, which is not surprising since we have incorporated their data in our fit. Their values for B and C of HS_2 (7996.378(23) and 7776.723(23) MHz, respectively) agree almost exactly with ours (see Table III). However, the value for A of 29 6974.403(32) MHz is 5 MHz smaller than ours. This is because they estimate a value for the centrifugal distortion parameter Δ_K of 19.7 MHz. Since we observe transitions with high K_a values, we have been able to determine that the correct value for Δ_K for HS_2 in its ground state is 24.339(10) MHz, significantly different from the previously assumed value. Because Yamamoto and Saito were able to determine only the quantity $(A + \Delta_K)$ from their measurements, this produces a similar error in the value for A also.

In a nonlinear free radical like HS_2, the orbital angular momentum is almost completely quenched and the fine structure splittings arise from second-order spin–orbit coupling effects which manifest themselves as spin–rotation coupling in the effective Hamiltonian (*17*). This interaction can be described predominantly by three diagonal

TABLE V

Molecular Parameters of the HS_2, HSO, and HO_2 Radicals in the (0, 0, 0) Vibrational Levels of Their Ground $\tilde{X}^2A''$ Electronic States

Parameter[a]	HO_2[b]	HSO[c]	HS_2[f]
A	610 273.223	299 484.63	296 979.060(13)[h]
B	33 517.816	20 504.56	7 996.3819(47)
C	31 667.654	19 133.93	7 776.7198(48)
Δ_N	0.11693	0.03070	0.00588684(62)
Δ_{NK}	3.44552	0.8960	0.233573(30)
Δ_K	123.572	27.2	24.339(10)
$\delta_N \times 10^3$	6.13	1.93	0.15580(28)
δ_K	2.017	0.89	0.1390(24)
$\Phi_{KN} \times 10^3$	1.051	...	0.321(12)
$\Phi_K \times 10^3$	9.69	...	8.68(61)
ϵ_{aa}	-49 571.409	-10 365.99	−45 926.824(34)
ϵ_{bb}	-422.755	-426.656	−424.0583(83)
ϵ_{cc}	8.605	0.226	9.8204(90)
$\frac{1}{2}\lvert\epsilon_{ab} + \epsilon_{ba}\rvert$	193.95	378.0	234.6966(49)
δ_K^s	0.079	...	...
Δ_K^s	23.061	2.953	6.429(22)
Δ_{NK}^s	0.1261	0.038	-0.06261(75)
$(0)_H$	-27.48[c]	-36.37	−22.60(15)
$(aa)_H$	-8.34[c]	-11.96	−5.98(15)
$(bb)_H$	19.74[c]	10.44	5.892(30)
$(ab)_H$	-18.3[c]	-7.8	-1.783(26)
g_S^{aa}	2.04204[d]	...	2.07809(47)
g_S^{bb}	2.00790[d]	...	2.0295(11)
g_S^{cc}	2.00152[d]	...	2.0013(11)
$g_r^{aa} \times 10^3$	-9.857[d]	...	−3.996(66)
$g_r^{bb} \times 10^3$	-1.85[d]	...	−0.54810
$g_r^{cc} \times 10^3$	...	...	−0.018476
r(H-X)	0.09974[c]	0.1494[c]	0.1352[i]
r(Y-X)	0.13339[c]	0.1389[c]	0.19606[i]
θ(HXY)	104.15[c]	106.6[c]	101.7[i]

[a] Parameter values given in MHz where appropriate.
[b] From Ref. (*11*).
[c] From Ref. (*22*).
[d] From Ref. (*23*).
[e] From Ref. (*12*).
[f] Present work.
[h] The figures in parentheses are one standard deviation of the least-squares fit in units of the last quoted decimal place.
[i] From Ref. (*7*).

components of the spin–rotation tensor, ϵ_{aa}, ϵ_{bb}, and ϵ_{cc} where a, b, and c denote the principal axes of inertia. For HS_2, an off-diagonal term, the average of ϵ_{ab} and ϵ_{ba}, is also required to describe certain energy levels (*16*). Hirota (*18*) gives a simplified expression for $\epsilon_{\alpha\alpha}$,

$$\epsilon_{\alpha\alpha} = 4A_{SO}B_\alpha \sum_n (-1)^{s_n} \frac{|\langle 0|L_\alpha|n\rangle|^2}{E(n) - E(0)}, \tag{3}$$

where the exponent s_n is even or odd depending on the type of excitation $0 \rightarrow n$. In HS_2, the axial (a) component of this tensor arises predominantly from coupling between the two Renner–Teller components deriving from the $^2\Pi$ state in the linear configuration, the $\tilde{X}\,^2A''$ and the $\tilde{A}\,^2A'$ states. Taking the values for A and ϵ_{aa} from Table III and the value of 7255 cm^{-1} for the $\tilde{X}$ to $\tilde{A}$ energy separation from Ref. (*4*) and assuming A_{SO} is the spin–orbit coupling constant for atomic sulfur (382 cm^{-1}, Ref. (*10*)), we obtain an estimate for the dimensionless quantity $|\langle 0|\, L_a |n\rangle|$ of 0.857. This value is somewhat smaller than the value of 1.0 expected for a Π state and can be attributed to the vibrational overlap factor being slightly less than unity.

The g-factors determined in the LMR experiment also carry information on the electronic structure of HS_2. For example, Curl (*19*) has shown that the anisotropy in the electron spin g_S tensor can be related to the components of the spin–rotation tensor

$$\Delta g_S^{\alpha\alpha} \equiv g_S^{\alpha\alpha} - g_e = \frac{-\epsilon_{\alpha\alpha}}{2B_\alpha}, \tag{4}$$

where g_e is the isotropic (free electron) value for the g-factor. The relationship can be tested for all three principal components of the $g_S^{\alpha\alpha}$ tensor from the present data. The results are given in Table IV, where it can be seen that the agreement is impressively good, perhaps because the spin–rotation tensor components are completely determined by off-diagonal spin–orbit coupling effects of the relatively heavy sulfur atoms.

One component of the rotational g-factor has also been determined: $g_\tau^{aa} = -0.3996(66) \times 10^{-2}$. This compares well with the value predicted by the formula given by Brown and Sears (*16*):

$$g_\tau^{aa} = \frac{\epsilon_{aa}}{\zeta_S} = -0.401 \times 10^{-2}. \tag{5}$$

The three analogous radicals, HO_2, HSO, and HS_2, have now been well characterized in their ground states. The molecular parameters for these species have been collected in Table V. The behavior of the parameter values through the series can be rationalized and interesting comparisons drawn. For example, the values for Δ_N (116.9, 30.7, and 5.89 kHz respectively) are very close to those for the corresponding diatomic molecules O_2, SO, and S_2 (145.1, 34.0, and 5.7 kHz, respectively (*20*)). This suggests that the A–B stretching force constant in the HAB molecule is very similar to that in the diatomic molecule AB. Again, the increased anisotropies in the electron spin g-factor g_S for HS_2 compared with HO_2 marks the increase in spin–orbit coupling in going from O (ζ = 151 cm^{-1}) to S (ζ = 382 cm^{-1}).

The HS_2 radical is now very well characterized in its ground $^2A''$ state. The molecule has also been detected in the next higher $\tilde{A}\,^2A'$ state (*5*). Very recently, better quality, higher resolution recordings of the $\tilde{A}\,^2A'$–$\tilde{X}\,^2A''$ system have been made (*21*). Work is now in progress on the analysis of this spectrum, using the results of the present paper and those of Ref. (*7*).

ACKNOWLEDGMENTS

We are very grateful to Lew Mullen for valuable technical assistance during the course of the experimental work. Professor Yamamoto kindly provided information about the millimeter-wave spectrum before publication. We also thank NIST for financial support of S.H.A.

RECEIVED: February 9, 1995

REFERENCES

1. J. T. HOUGEN, H. E. RADFORD, K. M. EVENSON, AND C. J. HOWARD, *J. Mol. Spectrosc.* **56,** 210–227 (1975).
2. K. V. CHANCE, K. PARK, K. M. EVENSON, AND L. R. ZINK, *J. Mol. Spectrosc.*, in press.
3. G. A. TAKACS AND C. J. HOWARD, *J. Phys. Chem.* **90,** 687–690 (1986).
4. G. PORTER, *Discuss. Faraday Soc.* **9,** 60–69 (1950).
5. K. J. HOLSTEIN, E. H. FINK, J. WILDT, AND F. ZABEL, *Chem. Phys. Lett.* **113,** 1–7 (1985).
6. A. B. SANNIGRAHI, S. D. PEYERIMHOFF, AND R. J. BUENKER, *Chem. Phys. Lett.* **46,** 415–421 (1977).
7. S. YAMAMOTO AND S. SAITO, *Can. J. Phys.* **72,** 954–962 (1994).
8. Q. ZHUO, D. CLOUTHIER, AND J. D. GODDARD, *J. Chem. Phys.* **100,** 2924–2931 (1994).
9. S. H. ASHWORTH AND J. M. BROWN, *J. Mol. Spectrosc.* **153,** 41–58 (1992).
10. K. M. EVENSON, *Faraday Discuss. Chem. Soc.* **71,** 7–14 (1981).
11. A. CHARO AND F. C. DE LUCIA, *J. Mol. Spectrosc.* **94,** 426–436 (1982).
12. Y. ENDO, S. SAITO, AND E. HIROTA, *J. Chem. Phys.* **75,** 4379–4384 (1981).
13. I. C. BOWATER, J. M. BROWN, AND A. CARRINGTON, *Proc. R. Soc. London Sect. A* **333,** 265–288 (1973).
14. A. CARRINGTON AND A. D. MCLACHLAN, "Introduction to Magnetic Resonance," p. 138, Harper & Row, New York, 1967.
15. J. T. HOUGEN, *J. Mol. Spectrosc.* **54,** 447–471 (1975).
16. J. M. BROWN AND T. J. SEARS, *J. Mol. Spectrosc.* **75,** 111–133 (1979).
17. J. H. VAN VLECK, *Rev. Mod. Phys.* **23,** 213–227 (1951).
18. E. HIROTA, *J. Phys. Chem.* **87,** 3375–3383 (1983).
19. R. F. CURL, *Mol. Phys.* **9,** 585–597 (1965).
20. K. P. HUBER AND G. HERZBERG, "Molecular Spectra and Molecular Structure, Vol. 4. Constants of Diatomic Molecules," Van Nostrand-Reinhold, New York, 1979.
21. E. H. FINK, private communication, 1993.
22. J. M. BROWN AND M. R. PURNELL, "Molecular Spectroscopy: Modern Research," Vol. III, p. 249, Academic Press, San Diego, 1985.
23. C. E. BARNES, J. M. BROWN, A. CARRINGTON, J. PINKSTONE, T. J. SEARS, AND P. J. THISLETHWAITE, *J. Mol. Spectrosc.* **72,** 86–101 (1978).